SANDIA REPORT

SAND2005-6004
Unlimited Release
Printed September 2005

Functionalized Nanoparticles for Sensor Applications

Kent Childs, Shawn Dirk, Stephen Howell, Robert J. Simonson and David Wheeler

Prepared by
Sandia National Laboratories
Albuquerque, New Mexico 87185 and Livermore, California 94550

Sandia is a multiprogram laboratory operated by Sandia Corporation,
a Lockheed Martin Company, for the United States Department of Energy's
National Nuclear Security Administration under Contract DE-AC04-94AL85000.

Issued by Sandia National Laboratories, operated for the United States Department of Energy by Sandia Corporation.

Available to DOE and DOE contractors from
U.S. Department of Energy
Office of Scientific and Technical Information
P.O. Box 62
Oak Ridge, TN 37831

Telephone: (865)576-8401
Facsimile: (865)576-5728
E-Mail: reports@adonis.osti.gov
Online ordering: http://www.osti.gov/bridge

Available to the public from
U.S. Department of Commerce
National Technical Information Service
5285 Port Royal Rd
Springfield, VA 22161

Telephone: (800)553-6847
Facsimile: (703)605-6900
E-Mail: orders@ntis.fedworld.gov
Online order: http://www.ntis.gov/help/ordermethods.asp?loc=7-4-0#online

SAND 2005-6004
Unlimited Release
Printed September 2005

Functionalized Nanoparticles for Sensor Applications

Kent Childs, Shawn Dirk, Stephen Howell, Robert J. Simonson, David Wheeler
Sandia National Laboratories
P.O. Box 5800
Albuquerque, New Mexico 87185-0892

ABSTRACT

We will describe our work on functionalized arrays of nanoparticles crosslinked with short conducting molecules that contain sensing functionalities. These bridging ligands modulate their conductivity based on their interaction with analytes. This functionalized nanoparticles organic ligand composite material once it is assembled between nanogaps electrodes will provide nanosized sensors that can be easily interrogated. These nanogap sensors will be engineered so that they can be fabricated into arrays of different sensor elements.

This project consists of a number of different requirements that must be met in order to enable the use of functionalized nanoparticles for sensor applications. The first requirement is the appropriately functionalized nanoparticle. The second is a method to assemble the particles. The third requirement is the generation of a nanogap to contain the nanoparticles.
The successes in each of these areas will be discussed as will the sensing behavior of the final films.

Contents

List of Figures

List of Tables

1. Introduction

1.1 Introduction and review of our approach*:*

Gold nanoparticles have been used for sensing applications. We propose to also employ metal nanoparticles for sensing applications but in a new and more sensitive format. We plan to assemble a small ensemble of nanoparticles between two nanoelectrodes. This will be achieved using demonstrated ac trapping or with our new surface chemistry. The ac trapping method will allow us to address single junctions from an array of junctions. Once the particles are in place, we will then stabilize the ensemble of particles using the surfactant (capping agent) replacement and crosslinking methodology that we have developed during the first year of our LDRD. With this methodology the capping agents on a nanoparticle can be completely or partially substituted with other tighter binding ligands. Once the ensemble is crosslinked it is possible to use the sensor in both liquid and gas sensing applications. To increase the sensitivity of ensemble, the crosslinking ligands will be pi-conjugated molecules with an analyte specific binding group or chemistry. By employing pi conjugated molecules to bridge the nanoparticles, the interparticle conduction mechanism will be dominated by the bridging ligand providing the remaining capping agent molecules are nonconductive and providing that the orbitals of the bridging ligand are energetically favorable for influencing electron transfer. Binding of an analyte molecule to one of the bridging ligands will change its charge transport properties as shown in Figure 1 below. This change in charge transport then can be measured electrically and an analyte concentration can be determined. The mechanism of impedance change is based on changes in the organic bridging molecules; this is fundamentally different than currently employed swelling mechanisms. Additionally, if there is a specific electrical response (perhaps a specific impedance change at a characteristic frequency or a distinctive IV curve) then there exists a built in verification or analyte identity check. The sensitivity of the device can be tuned by controlling the extent of the percolation path generated during the crosslinking step. A limited number of percolation paths would increase the sensitivity of the device, while an ensemble of particles with a large number of paths would respond a wider range of analyte concentrations before saturating. Employing identically functionalized sensors, but with different numbers of nanoparticles or nanoparticles crosslinking units, could improve the analyte discrimination and concentration determination and redundancy.

Small Particle Array
Limited Number of Communication Paths

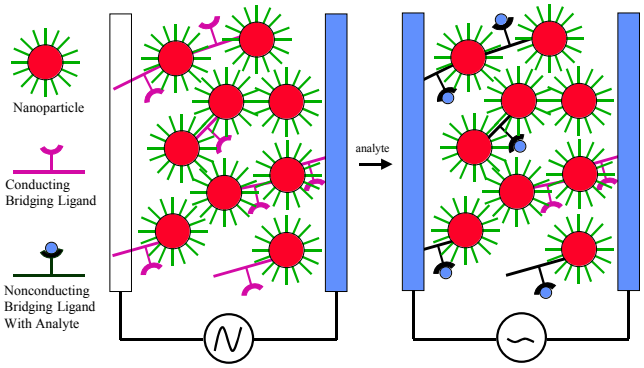

Figure 1 Analyte binging to pi conjugated bridging ligand reduces current flow and a signal transduction scheme.

This approach will rely both on a bottom up and a top down assembly to generate the needed density of sensor elements. Diazonium and iodonium salt based derivatization of surfaces forms the basis of the bottom up approach while the generation of the nanogap or crossbar architecture would require classic top down lithography. Typical methods of connection to other devices can be envisioned. Fault tolerance can be increased by redundancy of sensor elements each spanning a different concentration range (different degrees of crosslinking bridging elements) but still overlapping in range of response. Pattern recognition will provide an additional level of confidence to data analysis. The small pi conjugated bridging molecules are amendable to this approach and a large number of different ones can be imagined. Specifically, molecules that upon interaction with an analyte undergo a change will be examined. That change could be either a structural rearrangement, or and electronic rearrangement. We and others have demonstrated that electron deficient phenolic polymers reversibly bind phosphonates. Consequently, they will serve as our starting point. The changes in the electrical response of the hybrid organic/nanoparticle film will then be measured.

In this SAND report, we will discuss the breakthroughs that were needed for success. The descriptions will be in the form of papers that we have published and that we are in the process of submitting. In the first section we will discuss our nanoparticle synthesis that allows for rapid ligand replacement and cross linking. In the second section will describe the test nanogap structures that we built. In section three will address the functionalization chemistry that allows us to direct molecular assembly. In the final section we will describe our sensing results both aqueous and gas phase.

2. Synthesis of Pt and Au Nanoparticles with a Sacrificial Stearonitrile Shell

2.1 Platinum and gold nanoparticles were synthesized using stearonitrile as a capping agent, which may easily be displaced by stronger binding capping ligands.

Shawn M. Dirk, Stephen W. Howell, Rebecca Moorhouse, and David R. Wheeler*

Sandia National Laboratories[1], Albuquerque, USA. Fax: 505 845 8161; Tel: 505 844 6631; E-mail: drwheel@sandia.gov

Nanoparticles have received much attention and have been the subject of many reviews.[2] Nanoparticles have also been used to form super molecular structures for molecular electronic,[3] and sensor applications.[4] However, many limitations exist when using nanoparticles, including the ability to manipulate the particles post synthesis. Current methods to prepare nanoparticles employ functionalities like thiols,[5, 6] amines,[7] phosphines,[8] isocyanides,[9] or a citrate[10] as the metal capping agent. While these capping agents prevent agglomeration or precipitation of the particles, most are difficult to displace or impede packing in nanoparticle films due to coulombic repulsion. It is in this vein that we undertook the synthesis of nanoparticles that have a weakly bound capping agent that is strong enough to prevent agglomeration and in the case of the platinum particles allow for purification, but yet, easily displaced by other strongly binding ligands.

The nanoparticles where synthesized according to the Brust[1] method except stearonitrile was used instead of an aliphatic thiol. Both platinum and gold were examined in this manner. A representative procedure for the synthesis of platinum nanoparticles involved the phase transfer of chloroplatinic acid (0.37 g, 0.90 mmol) dissolved in water (30 mL) to a solution of tetraoctylammonium bromide (2.2 g, 4.0 mmol) in toluene (80 mL). After the chloroplatinic acid was transferred into the organic phase the aqueous phase was removed. Stearonitrile (0.23 g, 0.87 mmol) was added and sodium borohydride (0.38 g, 49 mmol) in water (25 mL) was added. The solution turned black almost immediately and after 15 min the organic phase was separated and passed through a 0.45 μm Teflon filter. The resulting solution was concentrated and twice precipitated into ethanol (~200 mL) to yield 0.11 g of black platinum nanoparticles. TGA experiments showed that the Pt particles contained 35 % by mass stearonitrile. TEM images showed an average particle size of 1.3 ± 0.3 nm shown in Figure 2.

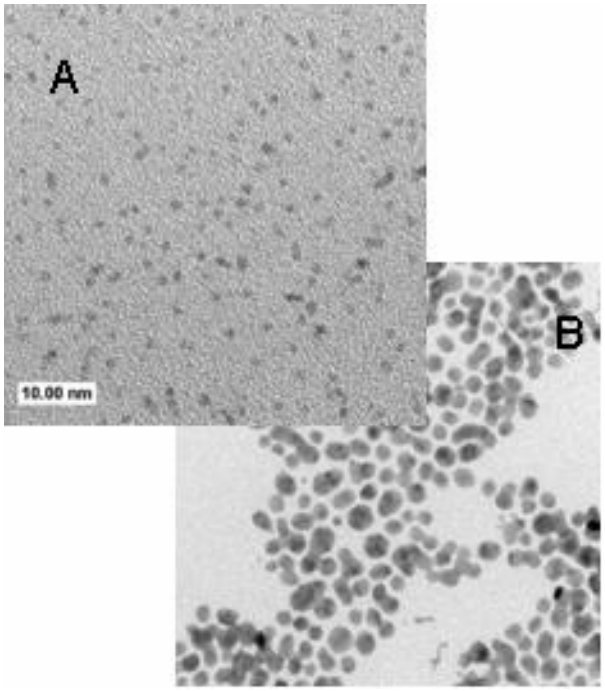

Fig. 2 (A) TEM image of stearonitrile-capped Pt nanoparticles drop-coated from toluene onto a TEM grid. (B) TEM image of stearonitrile-capped Au nanoparticles drop-coated from toluene onto a TEM grid.

A representative procedure for the synthesis of gold nanoparticles involved the transfer of hydrogen tetrachloroaurate (0.18 g, 0.53 mmol) dissolved in water (15 mL) to a solution of tetraoctylammonium bromide (1.1 g, 2.0 mmol) in toluene (40 mL). After the gold salt transferred into the organic phase the aqueous phase was removed. Stearonitrile (0.23 g, 0.87 mmol) was added and sodium borohydride (0.19 g, 5.0 mmol) in water (13 mL) was added. The solution turned dark red almost immediately, and after 15 min the organic phase was separated and passed through a 0.45 μm Teflon filter. The resulting solution was used without purification via precipitation because attempts at precipitation with ethanol resulted in agglomeration. TEM images showed an average particle size of 5.3 ± 1.3 nm shown in Figure 2.

The nanoparticles synthesized were also characterized using atomic force microscopy in tapping mode shown in Figure 2. The AFM images agree with the TEM images and show a relatively monodispersed collection of nanoparticles.

Platinum nanoparticles were synthesized without stearonitrile to show that the particles were in fact capped with the stearonitrile and not the tetraoctylammonium bromide. In the absence of stearonitrile the nanoparticles would not redissolve in

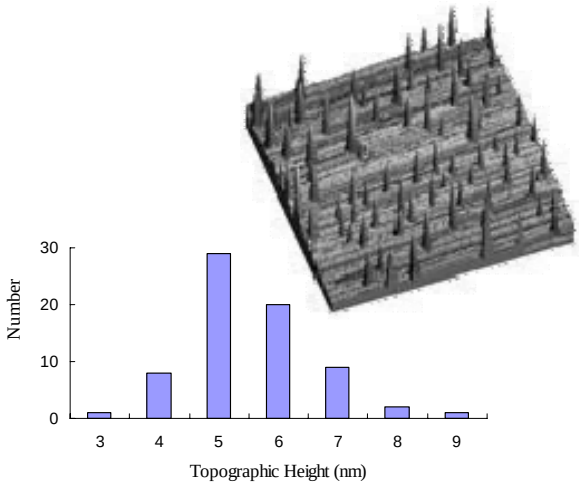

Fig. 3 Histogram of gold nanoparticles sizes with an AFM images of gold nanoparticles inlaid.

hexane or toluene after precipitation. While it is possible the tetraoctylammonium bromide helps prevent agglomeration by solvation into the capping stearonitrile ligand layer on the particles[11] recovery of a quantitative amount of the starting tetraoctylammonium bromide was difficult[12] and we cannot rule out that some small amount of tetraoctylammonium bromide serves in a synergistic capacity to help solubilize the isolated platinum particles.

Several exchange reactions were carried out using the isolated Pt nanoparticles. The stearonitrile cap was exchanged for hexadecylmercaptan, octanethiol, and benzeneethylthiol. In a typical exchange reaction, Pt nanoparticles (10 mg) were suspended in hexane (10 mL) and the exchange ligand was added (50µL). The solutions were allowed to stir overnight and

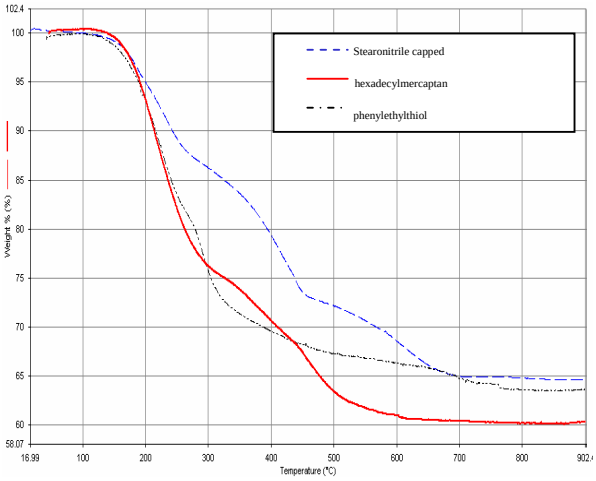

Fig. 4 TGA data from exchange reactions.

precipitated twice using ethanol. TGA experiments confirmed ligand exchange.

We have also shown that these particles may be assembled in a layer by layer (LBL) fashion to build up three dimensional assemblies. As an example of this LBL assembly a substrate consisting of gold electrodes separated by 8 µm on a quartz wafer was first functionalized by immersing in a solution of 1,8-octanedithiol (50 µL) in hexane (10 mL) for 15 min, rinsed with hexane (10 mL), ethanol (10 mL), and dried under a stream of nitrogen. The scaffold was then placed in a toluene solution containing Au nanoparticles capped with stearonitrile (10 mg/mL) for 15 minutes. The scaffold was then rinsed with hexane (10 mL), ethanol (10 mL), and dried under a stream of nitrogen. The substrate was then immersed iteratively between the 1,8-octanedithiol and the Au nanoparticle solution 4 more times. The assembly was characterized by AFM as shown in Figure 5.

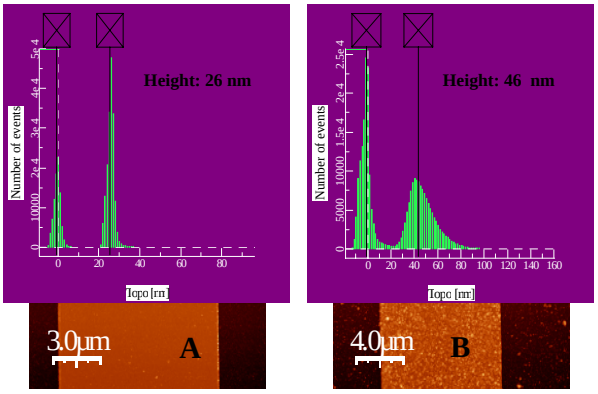

Fig. 5 (A) AFM image of a gold line on a quartz wafer before assembly. (B) AFM image of a gold line on a quartz wafer after 5 iterations of 1,8-octanedithol and Au nanoparticles.

According to the AFM data obtained, the assembly process resulted in a mean height increase of 20 nm (57% of theoretical). We believe the wide distribution observed in height after assembly is in part due to the fact that the Au nanoparticles used for assembly purposes were not purified via precipitation (as mentioned above). As a result entrained tetraoctylammonium bromides salts result in culombic repulsion and slightly inhibit assembly.

In conclusion we have synthesized Pt and Au nanoparticles containing an easily displaceable stearonitrile capping agent. The Pt particles are easily purified by precipitation and both The Au particles were assembled without purification in an iterative fashion and resulted in a wide distribution of height increase. It is the belief of the authors that the Pt nanoparticles are ideally suited for use in assembly purposes due to the fact that they may be purified and are capped with the easily displacable stearonitrile.

References

1 Sandia is a multiprogram laboratory operated by Sandia Corporation, a Lockheed Martin Company, for the United States Department of Energy's National Nuclear Security Administration under contract DE-AC04-94AL85000.

2 A. C. Templeton, W. P. Wuelfing, and R. W. Murray, A*cc. Chem. Res.,* 2000, **33,** 27.

3 J. H. Fendler, C*hem. Mater.,* 2001, **13,** 3196; D. J. Schiffrin, M*RS Bulletin,* 2001, **26,** 1015.

4 (A) H. Wohltjen and A. W. Snow, A*nal. Chem.,* 1998, **70,** 2856. (B) H. L. Zhang, S. D. Evans, J. R. Henderson, R. E. Miles, and T. H. Shen, *Nanotechnology,* 2002, **13,** 439. (C) C. R. Raj, T. Okajima, and T. Ohsaka, *Journal of Electroanal. Chem.,* 2003, **543,** 127.

5 M. Brust, J. Fink, D. Bethell, D. J. Schiffrin, and C. Kiely, J. *Chem. Soc. Chem. Comm.,* 1995, 1655.

6 S. Chen and R. W. Murray, L*angmuir,* 1999, **15,** 682.

7 (A) S. Mandal, P. R. Selvakannan, D. Roy, R. V. Chaudhari, and M. Sastry, C*hem. Comm.,* 2002, 3002. (B) P. R. Selvakannan, S. Mandal, R. Pasricha, S. D. Adyanthaya, and M. Sastry, C*hem. Comm.,* 2002, 1334.

8 (A) W. W. Weare, S. M. Reed, M. G. Warner, and J. E. Hutchison, *J. Am. Chem. Soc.,* 2000, **122,** 12890. (B) B. L. V. Prasad, S. I. Stoeva, C. M. Sorensen, and K. J. Klabunde, C*hem. Mater.,* 2003, **15,** 935.

9 (A) S. L. Horswell, C. J. Kiely, I. A. O'Neil, and D. J. Schiffrin, J. *Am. Chem. Soc.,* 1999, **121,** 5573. (B) H. S. Kim, S. J. Lee, N. H. Kim, J. K. Yoon, H. K. Park, and K. Kim, L*angmuir,* 2003, **19,** 6701.

10 B. V. Enustun and J. Turkevich, *J. Am. Chem. Soc.,* 1963, **85,** 3317.

11 C. A. Waters, A. J. Mills, K. A. Johnson, and D. J. Schiffrin, C*hem. Comm.,* 2003, 540.

12 Recovery of the tetraoctylammonium bromide was difficult due to adventitious stearonitrile. In addition, the high heat that was required to dry the ammonium salt resulted in decomposition.

INSTITUTE OF PHYSICS PUBLISHING NANOTECHNOLOGY
Nanotechnology **16** (2005) 754–758 doi:10.1088/0957-4484/16/6/022

3. Mass-fabricated one-dimensional silicon nanogaps for hybrid organic/nanoparticle arrays

Stephen W Howell[1], Shawn M Dirk[1], Kenton Childs[2], Harry Pang[3], Matthew Blain[1], Robert J Simonson[1], James M Tour[3] and David R Wheeler[1,4]

[1] Micro Analytical Systems Department, Sandia National Laboratories, Albuquerque, NM 87185, USA
[2] Rad Hard CMOS Technology Department, Sandia National Laboratories, Albuquerque, NM 87185, USA
[3] Department of Chemistry and Center for Nanoscale Science and Technology, Rice University, MS 222, 6100 Main Street, Houston, TX 77005, USA

E-mail: drwheel@sandia.gov

Received 22 December 2004, in final form 22 February 2005
Published 5 April 2005
Online at stacks.iop.org/Nano/16/754

Abstract
Optical lithography based on microfabrication techniques was employed to fabricate one-dimensional nanogaps with micrometre edge lengths in silicon. These one-dimensional nanogaps served as a platform on which organic/nanoparticle films were assembled. Characterization of the gaps was performed with high-resolution TEM, SEM, and electrical measurements. Novel self-assembling attachment chemistry, based on the interaction of silicon with a diazonium salt, was used to iteratively build a multi-layer nanoparticle film across a 7 nm gap. By using nanoparticles capped with an easily displaced ligand, a variable conductive path was created across the 1D nanogap. Electrical measurements of the gap showed a dramatic change in the $I(V)$ characteristics after assembly of the nanoparticle film.

(Some figures in this article are in colour only in the electronic version)

3.1 Introduction

Recently, films composed of nanoparticles suspended in a matrix of organic ligands have emerged as a useful platform for chemical and biological sensing [1–4]. The mechanism of signal transduction described in these initial reports was primarily based on swelling of a film of nanoparticles suspended in an organic matrix. A potential improvement on this mechanism would be to cross-link the nanoparticles with ligands possessing analyte-binding sites. Analytes could be detected through electrical transduction if the binding event modified the organic scaffold making the cross-linking molecule more or less conductive, provided that the organic molecules play a role in charge transport.

To take full advantage of the organic/nanoparticle system, an electrode geometry is desired with the shortest possible path length through the film from one contact to the next. With this configuration, the resulting measured conductance of the organic/nanoparticle composite film is an average over a relatively low number of organic/metal junctions. Thus, any modification due to changes in the conduction of the linker molecules can be more easily detected. Built-in redundancy can be achieved by combining multiple short electrode–film–electrode percolation paths into a parallel configuration. Given the methodology discussed above, a contact electrode configuration with a nanometre-scale gap that is several micrometres long is a desirable platform on which to deposit an organic/nanoparticle film.

Over the past decade, many novel techniques have appeared in the literature for the fabrication of three-dimensional nanogaps [5–14]. Although interesting and often effective, most of those techniques are not easily amenable to mass production. Previous nano-fabrication methods

[4] Author to whom any correspondence should be addressed.

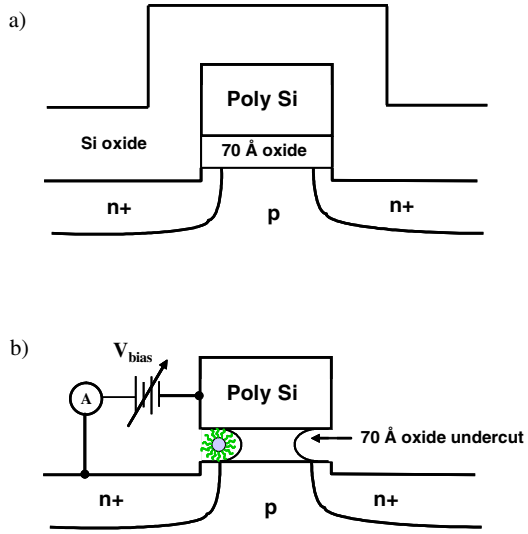

Figure 6. Cross-sectional device schematic: (a) before etch of passivation oxide; (b) after oxide etch and assembly of organic/nanoparticle film.

rely primarily on the technologies and techniques of AFM lithography [5–7], E-beam lithography [8–10, 15], break junctions [14], molecular imprinting [16] and electrochemical methods [11, 12]. However, since many of these techniques often rely on serial-raster-write approaches, fabrication of large numbers of dense electrode arrays will be expensive and time consuming. One novel fabrication technique that has recently been reported is to use chemical mechanical polishing (CMP) to produce nanometre gaps that have a micrometre lateral dimension [13]. Although fabrication of these nanogaps is relatively simple, the geometry makes control of the leakage current through the gap difficult. Our geometry here offers advantages such as reduced leakage currents through the thin oxide due to our angled implant (see below). Another recent reports demonstrate how metallic 1D nanogaps can be fabricated using novel conventional lithography and molecular-beam epitaxy [17–19]. These reports clearly show how standard lithography can be used to fabricate 1D metallic nanogaps that can be functionalized with various attachment chemistries. However, to our knowledge there have been no reports of 1D silicon nanogaps fabricated by a conventional lithography that can be easily functionalized.

In order for organic/nanoparticle-film based sensors to become practical, techniques for fabricating nanogaps must be developed that are amenable to mass production. We have developed a novel fabrication technique for producing arrays of silicon 1D nanogaps based on standard optical lithography and CMOS processing. Our process allows for the accurate mass fabrication of gaps in a range from 2–100 nm, making it a useful platform to measure the electrical transduction of organic/nanoparticle films suspended between the electrode gaps. Our fabrication method generates 1D nanogaps with silicon electrodes, thereby avoiding metal filament formation, which can plague nanogaps fabricated with metal electrodes [20]. We first discuss the fabrication and characterization of the 1D nanogaps. Next, results from a proof of principle experiment will be described, wherein assembly of an organic/gold nanoparticle film across a 7 nm silicon–

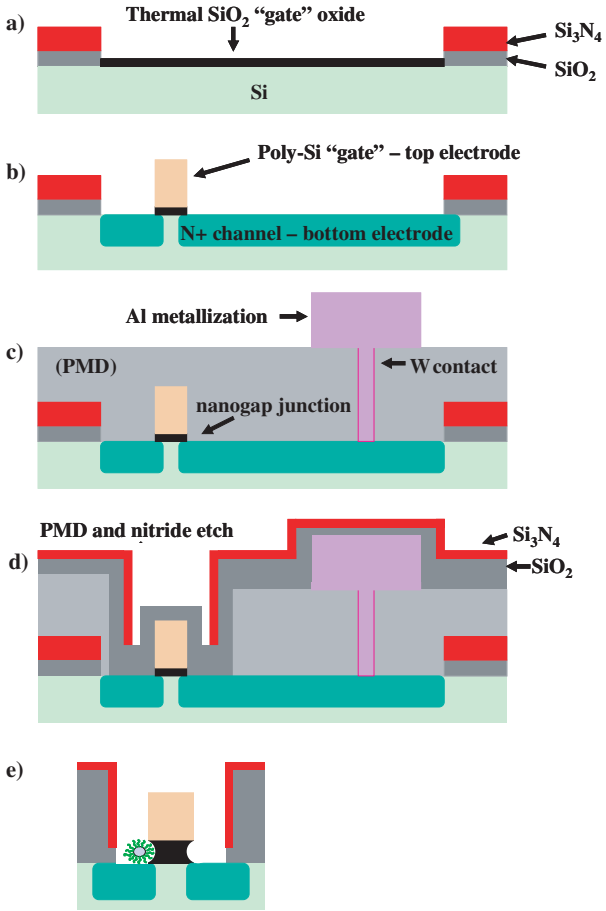

Figure 7. ((a)–(d)) Fabrication process for the Si nanogap device. (e) Functionalization of the device after removal of the passivation oxide.

silicon gap caused significant changes in the two-electrode $I(V)$ characteristics.

3.2 Device fabrication

Standard CMOS processing steps were used to fabricate addressable 1D nanogaps in Si, as schematically illustrated in figure 1. The active, two-terminal device is formed within the gate module. The top electrode consists of the poly-Si gate and the bottom electrode is a highly doped N+ channel in the Si substrate. The nanogap width was determined by the thickness of the thermally grown gate oxide, and can therefore be controlled over a wide range of values.

Figure 7 illustrates the device fabrication process. A 15 nm SiO_2 pad was grown on a p-type Si substrate followed by deposition of 100 nm Si_3N_4. The nitride and oxide were patterned for the eventual heavy dose Arsenic implant, which provides the lower electrode of the two-terminal device. This was followed by the growth of a thin 'gate' SiO_2, the thickness of which determines the active nanogap width. This cross-sectional structure is illustrated in figure 2(a). Polycrystalline Si (poly-Si) was then deposited, implanted and patterned, forming the top electrode. The heavy dose Arsenic implant defined the lower electrode using a 10° tilt and quad rotation in order to bring the N+ electrode just under the edge of

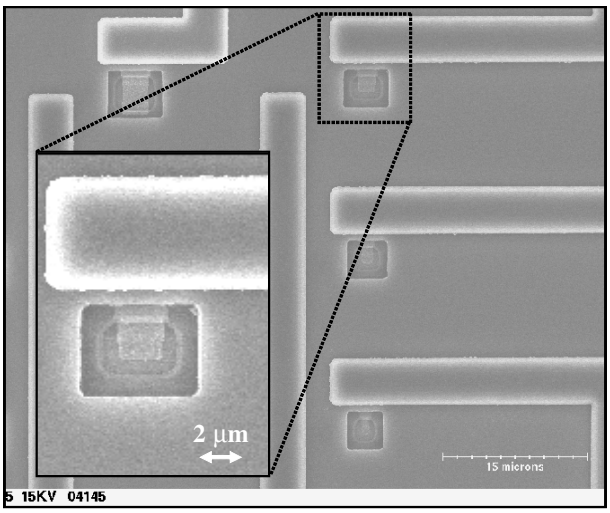

Figure 8. SEM image of multiple nanogap devices.

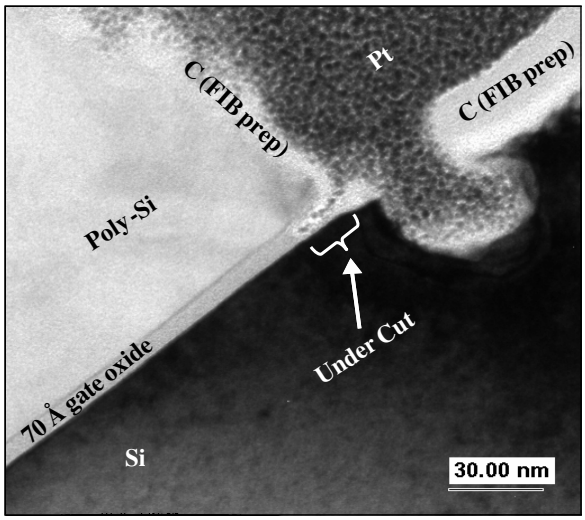

Figure 9. High-resolution TEM cross-section of a fabricated 7 nm gap showing the undercut of the spacer oxide. Note that C and Pt were deposited as a part of the TEM sample preparation.

the poly-Si top electrode, figure 7(b). Consequently, the poly-Si gate acts as an implant mask, limiting the overlap of the top and bottom electrodes to the edge of the poly-Si and minimizing the leakage current from the central area of the poly-Si electrode through the thin SiO_2 to the p-type substrate. SiO_2 was deposited and planarized to form the pre-metal dielectric (PMD). Tungsten plugs provide electrical contacts from standard Al(Cu) metallization through the PMD to both the poly-Si top electrode and the N+ bottom electrode, figure 2(c). The two-electrode structure was exposed by opening the PMD. 300 nm SiO_2 and 100 nm Si_3N_4 films were blanket-deposited to provide a top passivation layer. The top Si_3N_4 layer was patterned and etched exposing the 300 nm SiO_2 passivation for subsequent opening to the bond pads and the two-electrode structures, figure 2(d). To bridge the electrode gap with organic/nanoparticle films, the 300 nm passivation oxide was removed and the gate oxide was undercut in a buffered oxide etch (BOE). An organic/nanoparticle film was then assembled across the resulting gap (figure 2(e)). While devices with nanogaps from 2 to 15 nm were fabricated, this paper describes the results from devices with a 7 nm gap bridged by an organic/gold nanoparticle film.

The layout of multiple devices is shown in figure 3. This layout includes poly-Si electrodes of differing edge lengths. Note that the organic self-assembled monolayer (SAM) coatings will only be active where the lower N+ electrode intersects the edges of the top poly-Si electrode. Thus, these devices differ in the active edge length. Ideally, the signal from a functionalized device should be proportional to the active edge length.

In addition to the structures in which the PMD and the passivating nitride layers were opened, the same structures were fabricated with no etched openings in the PMD or nitride layers. These unopened structures served as reference devices, whose conductivity should not change with post-fabrication BOE etch or SAM coating steps.

3.3 Post fabrication device characterization

To protect the silicon nanogaps during the dicing phase of fabrication, the active gap area was passivated with SiO_2, as previously described. To use the gap, the passivation oxide was removed with a buffered oxide etch (BOE). High-resolution cross-sectional transmission electron microscopy (TEM) was used to examine the gaps before and after removal of the passivation oxide. TEM was also used to examine the quality of the dielectric used to isolate the Si electrodes. Figure 4 displays a TEM image of the gap after a 60 s exposure to 6:1 BOE (Riedel-deHaën). The presence of Pt between the poly-Si and Si in the cross-sectional image clearly shows the formation of an undercut electrode.

Electrical characterization was conducted on the various edge length devices to determine how the geometry of the Si electrodes affects leakage current through the gap (figure 1(b)). The electrical characterization indicated that, for the 7 nm gate oxide devices, the leakage was dominated by the breakdown of the gate oxide, which typically occurred at bias voltages greater than ± 7 V. Note that this corresponds to a breakdown field of 10 MV cm^{-1}, consistent with an excellent quality thermal oxide. For bias voltages below ± 7 V, the maximum leakage was typically found to be <1 pA.

3.4 Experimental details

After determining the conditions required to reproducibly clear the active devices of passivation oxide, a simple experiment was conducted to test the effectiveness of the fabricated 1D nanogaps. To test the Si nanogap concept, a multilayered film of Au nanoparticles and organic cross-linking molecules was assembled (see below) in the active area of opened 7 nm 1D nanogap devices that had the same poly-Si electrode configuration as shown in the inset on figure 8.

3.4.1 Sample preparation

The passivating oxide covering the active area of the device was opened by immersing in a 6:1 buffered oxide etch solution for 1 min, then rinsed with deionized water for $\sim$30 s and finally dried under a stream of nitrogen. The devices were

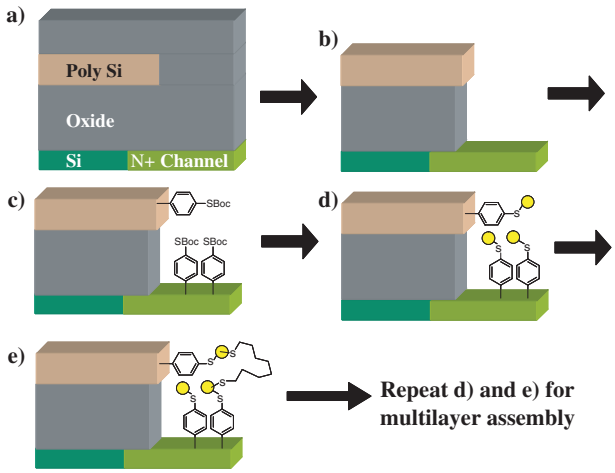

Figure 10. The nanogap functionalization process. (a) Before oxide removal. (b) Exposure to 6:1 BOE for 1 min. (c) 4-*tert*-butoxycarbonylsulfanyl–benzenediazonium; tetrafluoro borate (1 mmol ml^{-1}) in acetonitrile incubated for 45 min. TFA (5 drops) in methylene chloride (10 ml) for 10 min. (d) 5 nm Au nanoparticles capped with dodecylamine (4 mg) in toluene (10 ml) for 5 min. (e) 1,8-octanedithiol (50 μl) in toluene (10 ml) for 5 min. For these experiments, a multi-layered film was deposited by repeating steps (d) and (e) 5 times.

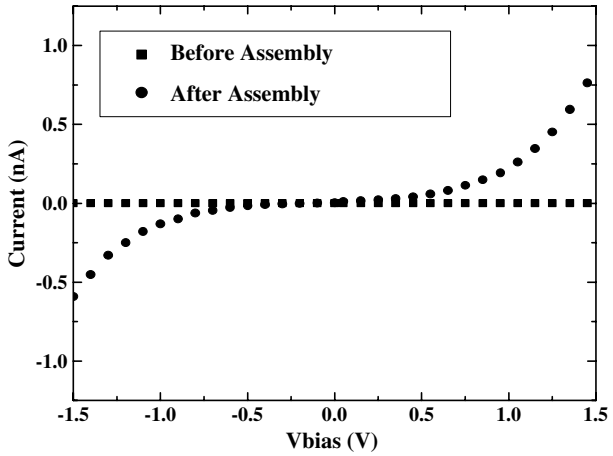

Figure 11. $I(V)$ data before and after the gap is functionalized with a nanoparticle film.

then tested prior to assembly to assure the presence of an open gap. Following testing, the devices were incubated in a solution of 4-*tert*-butoxycarbonylsulfanyl–benzenediazonium tetrafluoroborate (2.0 mg) in acetonitrile (10 ml) under argon for 40 min [21]. Upon removal from the diazonium assembly solution, the device was rinsed with acetonitrile (∼30 s) and ethanol (∼30 s) and dried under a stream of nitrogen. The thiol was then unmasked by immersing the substrate in a solution of trifluoroacetic acid (5 drops) dissolved in methylene chloride (10 ml) for 10 min. After deprotection, the part was rinsed with methylene chloride and ethanol and dried under a stream of nitrogen.

The thiol-functionalized device was then immersed for 5 min in a solution of either 5 nm diameter dodecylamine [22] capped or stearonitrile [23] capped Au nanoparticles (2.0 mg) in toluene (10 ml). Following the incubation with Au nanoparticles, the assembly was rinsed with toluene, ethanol and then dried under a stream of nitrogen. After the Au nanoparticle assembly, the device was incubated in a solution of 1,8-octanedithiol (50 μl) dissolved in toluene (10 ml) for 5 min then rinsed with toluene, ethanol, and dried under a stream of nitrogen. For these experiments, the nanoparticle and dithiol immersions were repeated until five layers were deposited, as shown in figure 10.

3.4.2. Electrical measurements

The first step in the procedure for probing the 7 nm devices was to measure the $I(V)$ characteristics just after removal of the passivation oxide. This step was important for avoiding defective devices. After the initial characterization, the devices were then functionalized with the nanoparticle film using the process described above. The electrical characteristics of these same devices were then measured immediately after the assembly. All measurements were made in ambient environmental conditions. Control experiments employing solvents without the assembly reagents or nanoparticles did not change the $I(V)$ characteristics of the device, substantiating that the changes in $I(V)$ characteristics are due to the organic/nanoparticle film.

Figure 6 displays a typical $I(V)$ curve for a 7 nm gap device with an active edge length of 4 μm before and after assembly of an organic/gold nanoparticle film. Before assembly, the $I(V)$ curves showed very little or no bias voltage dependence below the threshold voltage for breakdown. The maximum current in this voltage-gap region was typically <1 pA. There was a clear change in the $I(V)$ characteristic of the device after assembly of the organic/gold nanoparticle film.

After assembly, there was a strong current dependence on the applied bias voltage and the magnitude of the current increased by several orders of magnitude, to the nanoampere range. This clearly showed a modification of the conduction across the gap, and implies the bridging of the 7 nm gap with a conducting organic/gold nanoparticle film. The observed nonlinear $I(V)$ could be due to several factors. One possibility is that since the gap is only 7 nm wide and bridged by only five organic/metal junctions, the voltage drop across each ligand–nanoparticle junction is large enough to reveal more individual $I(V)$ characteristics of the linking ligands. A more likely explanation is that a Schottky-like barrier may exist where the diazonium attachment chemistry is bound to the implanted Si electrode. The origin of the observed nonlinear shape of the $I(V)$ curve is under investigation.

Several high-voltage sweeps (−8 to +8 V) were applied across the gap of a device which had been previously functionalized. Figure 12 displays the $I(V)$ curves from consecutive voltage sweeps. These data show that after each sweep the magnitude of the current for a particular voltage decreases. The cause of this degradation is not yet understood, but is likely related to the high-voltage sweeps. For the low-bias experiments ($V_{\text{bias}} < 2$ V), the film was resilient over multiple sweeps. Using more refractory metals such as palladium may extend the lifetime of these systems at higher voltages.

The yield of functionalized devices was found to be 80–90% after screening for defective post-fabrication

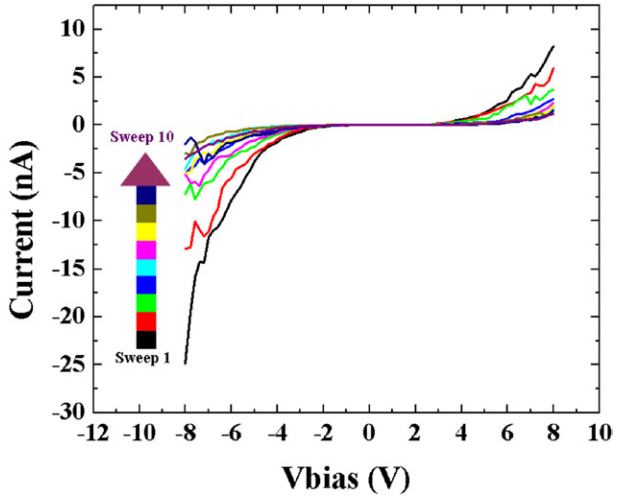

Figure 12. Consecutive $I(V)$ sweeps of a nanoparticle film bridging a 7 nm gap. These data show a degradation of the film over time.

parts. To our knowledge, there has been only one report describing functionalization of nanogaps with comparable high yields [15].

3.5 Conclusion

In summary, we have fabricated a simple Si 1D nanogap platform for monitoring the electrical behaviour of nanoparticle films. Devices with gaps of 2, 4 and 7 nm were fabricated. Cross-sectional TEM imaging revealed the formation of well defined gaps after the removal of the passivating oxide. The 7 nm gap devices were found to show a considerable increase in current after they were functionalized with an organic/gold nanoparticle film. The functionalized gaps were found to be more resilient for bias sweeps <2 V than larger sweeps of ± 8 V. This simple proof-of-principle experiment demonstrated how 1D gaps could serve as useful platform for electrical characterization of organic/nanoparticle films.

Acknowledgments

The authors thank Sherry Zmuda and Michael Stewart for their useful discussions. Sandia is a multiprogram laboratory operated by Sandia Corporation, a Lockheed Martin Company, for the United States Department of Energy under contract DE-AC04-94AL85000. The work at Rice University was supported by the Defense Advanced Research Projects Agency and the Office of Naval Research.

References

[1] Yu A M, Liang Z J, Cho J H and Caruso F 2003 *Nano Lett.* **3** 1203–7
[2] Lewis N S, Doleman B J, Briglin S and Severin E J 2003 *US Patent Specification* 6537498, pp 24 Cont.-in-part of U.S. Ser. No. 986,500
[3] Wohltjen H and Snow A W 1998 *Anal. Chem.* **70** 2856–9
[4] Zhang H L, Evans S D, Henderson J R, Miles R E and Shen T H 2002 *Nanotechnology* **13** 439–44
[5] Irmer B, Kehrle M, Lorenz H and Kotthaus J P 1997 *Appl. Phys. Lett.* **71** 1733–5
[6] Matsumoto K, Gotoh Y, Maeda T, Dagata J A and Harris J S 2000 *Appl. Phys. Lett.* **76** 239–41
[7] Snow E S, Campbell P M, Rendell R W, Buot F A, Park D, Marrian C R K and Magno R 1998 *Semicond. Sci. Technol.* **13** A75–8
[8] Guillorn M A, Carr D W, Tiberio R C, Greenbaum E and Simpson M L 2000 *J. Vac. Sci. Technol.* B **18** 1177–81
[9] Lefebvre J, Radosavljevic M and Johnson A T 2000 *Appl. Phys. Lett.* **76** 3828–30
[10] Lambert M F, Goffman M F, Bourgoin J P and Hesto P 2003 *Nanotechnology* **14** 772–7
[11] Yun M H, Myung N V, Vasquez R P, Lee C S, Menke E and Penner R M 2004 *Nano Lett.* **4** 419–22
[12] Mbindyo J K N, Mallouk T E, Mattzela J B, Kratochvilova I, Razavi B, Jackson T N and Mayer T S 2002 *J. Am. Chem. Soc.* **124** 4020–6
[13] Lee C, Yang E-H, Myung N V and George T 2003 *Nano Lett.* **3** 1339–40
[14] Reed M A, Zhou C, Muller C J, Burgin T P and Tour J M 1997 *Science* **278** 252–4
[15] Yu L H and Natelson D 2004 *Nano Lett.* **4** 79–83
[16] Austin M D, Ge H, Wu W, Li M, Yu Z, Wasserman D, Lyon S A and Chou S Y 2004 *Appl. Phys. Lett.* **84** 5299–301
[17] Choi J, Lee K and Janes D B 2004 *Nano Lett.* **4** 1699–703
[18] Natelson D, Willett R L, West K W and Pfeiffer L N 2000 *Appl. Phys. Lett.* **77** 1991–3
[19] Krahne R, Yacoby A, Shtrikman H, Bar-Joseph I, Dadosh T and Sperling J 2002 *Appl. Phys. Lett.* **81** 730–2
[20] Lau C N, Stewart D R, Williams R S and Bockrath M 2004 *Nano Lett.* **4** 569–72
[21] Stewart M P, Maya F, Kosynkin D V, Dirk S M, Stapleton J J, McGuiness C L, Allara D L and Tour J M 2004 *J. Am. Chem. Soc.* **126** 370–8
[22] Krasteva N, Guse B, Besnard I, Yasuda A and Vossmeyer T 2003 *Sensors Actuators* B **92** 137–43
[23] Dirk S M, Howell S W, Moorhouse R A and Wheeler D R 2005 *Chem. Lett.* submitted

INSTITUTE OF PHYSICS PUBLISHING NANOTECHNOLOGY
Nanotechnology **16** (2005) 1983–1985 doi:10.1088/0957-4484/16/10/001

4.Novel one-dimensional nanogap created with standard optical lithography and evaporation procedures

Shawn M Dirk[1], **Stephen W Howell**[1], **Sherry Zmuda**[1], **Kenton Childs**[2], **Matthew Blain**[1], **Robert J Simonson**[1] and **David R Wheeler**[1,3]

[1] Micro Analytical Systems Department, Sandia National Laboratories, Albuquerque, NM 87185, USA
[2] Rad Hard CMOS Technology Department, Sandia National Laboratories, Albuquerque, NM 87185, USA

E-mail: drwheel@sandia.gov

Received 24 June 2005
Published 3 August 2005
Online at stacks.iop.org/Nano/16/1983

Abstract
This article details a simple four-step procedure to create a one-dimensional nanogap on a buried oxide substrate that relies on conventional photolithography performed on a stack of silicon/silicon oxide/silicon, metal evaporation, and hydrofluoric acid oxide removal. Once the nanogap was fabricated it was bridged with an assembly of 1,8-octanedithiol and 5 nm Au nanoparticles capped with a sacrificial dodecylamine coating. Before assembly, characterization of the nanogaps was performed through electrical measurements and SEM imaging. Post assembly, the resistance of the nanogaps was evaluated. The current increased from 70 fA to 200 μA at +1 V bias, clearly indicating a modification due to nanoparticle molecule assembly. Control experiments without nanoparticles or octanedithiol did not show an increase in current.

4.1 Introduction

As the fields of molecular electronics and molecular sensors advance, the ability to efficiently produce a high fidelity nanogap is becoming paramount in order to facilitate our understanding of molecular interfaces and molecule–nanoparticle interactions. Several recent publications have addressed the need for nanogaps, and presented methods of fabrication including mechanical break junctions [1, 2], electromigration [3], nanoscale break junctions [4], nanopore [5], e-beam fabricated [3, 6–8], electrochemical deposition [9, 10], angled evaporations [11], and transistor-type devices containing SAM (self-assembled monolayers) cuts [12].

These techniques all result in usable nanogaps for molecular electronic and sensing applications. Here we present an alternative to the aforementioned methods of fabrication, suitable for implementation into back-end fabrication processing. This article presents a simple, high-yield, test structure that was fabricated in only four steps. All of the processing can be done in a typical clean room. Once fabricated, the nanogaps were characterized both with electron microscopy and with electrical measurements. After full characterization the nanogaps were functionalized in an iterative fashion using 1,8-octanedithiol and 5 nm Au nanoparticles capped with a sacrificial dodecylamine layer [13]. The devices were electrically analysed again following functionalization.

4.2 Device fabrication

The nanogaps were formed from a SOITECH 150 mm silicon-on-insulator (SOI) wafer that was composed of a 250 nm top single-crystal silicon layer on 170 nm buried silicon oxide

[3] Author to whom any correspondence should be addressed.

0957-4484/05/101983+03$30.00

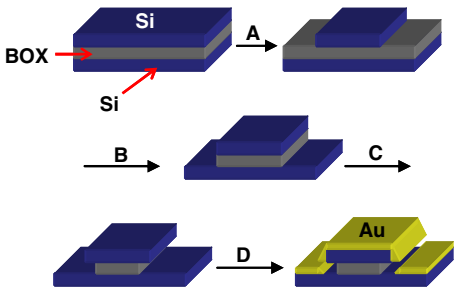

Figure 13. The process used to form nanogaps from an SOI wafer includes: (A) etching the 'top' single-crystal silicon, (B) etching the buried oxide, (C) wet etching in order to undercut the buried oxide, (D) evaporating Au.

(This figure is in colour only in the electronic version)

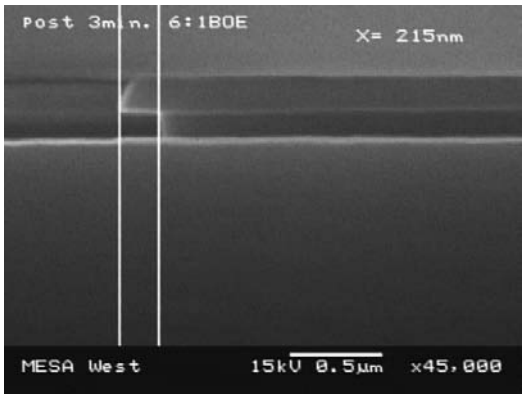

Figure14. SEM cross-section of the undercut BOX formed by 6:1 BOE etch, prior to Au evaporation.

(BOX) layer. The process by which the nanogaps were formed is depicted in figure 13.

The first step in nanogap formation involved a photolithography process to pattern a terrace structure on the SOI wafer (this step defined the top contact area as well as the edge length). In this case all edge lengths were between 792 and 968 μm. The structures were then plasma etched to clear 250 nm of single-crystal silicon, stopping on the BOX. Following the Si etch, the 170 nm BOX layer was defined by dry etching down to the substrate silicon using the same lithography pattern. The wafers were stripped of photoresist and cleaned using acetone and isopropyl alcohol. The buried oxide was then partially undercut by performing a wet etch in 6:1 buffered oxide etch (BOE) for 3 min under constant agitation, then rinsed in deionized water (DI) H_2O for 10 min. A 100 nm recess of the oxide was achieved, based on SEM cross-section analysis; see figure 14. The part was dried with an N_2 gun and placed immediately into a metal evaporator.

Metal evaporation was performed in a Temescal e-beam, semi-automated, evaporation system. Great care was taken to mount the terraced substrate directly over the centre of the crucible, normal to the source, rather than at the usual 10° angle on the orbital fixture. The sample was rotated about the axis during the entire evaporation. An adhesion layer, 10 nm titanium, was deposited onto the entire part, followed by a 90 nm Au layer. Post-evaporation SEM measurements on cross-sections showed that approximately 110 nm of metal had been evaporated onto the part, forming a 60 nm gap as shown in figure 15.

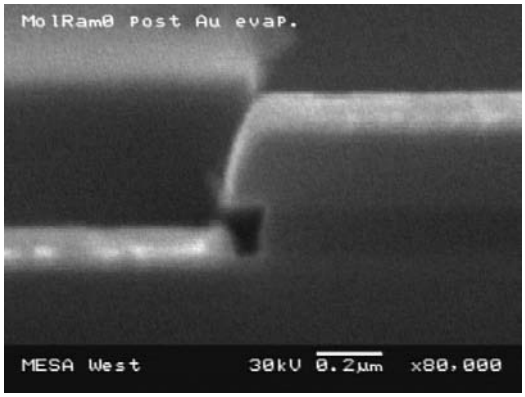

Figure 15. SEM image after the substrate was cleaved, showing the Au evaporation forming the nanogap.

4.3 Post fabrication device characterization

Since the 1D nanogap was designed to have nanoparticles and molecules assembled across the gap it was important to characterize the device completely before any subsequent assembly of organic and inorganic materials. Prior to electrical characterization the device was first cleaned in a piranha solution (1:1) for 5 min, rinsed with DI H_2O, dried under a stream of nitrogen and examined electrically using a Hewlett Packard Semiconductor Parameter Analyzer Model 4156A. The voltage was swept from 0 to +1 V to −1 to 0 V in 10 mV steps to minimize electrostatic induced shock. The measurements were made using a probe station with tungsten probe tips.

4.4 Experimental details

4.4.1. Sample preparation

After electrical characterization, the substrate was placed in a solution of octanedithiol (25 μl) dissolved in toluene (10 ml) and incubated for 10 min. After incubation, the substrate was rinsed with toluene, followed by ethanol, and then dried under a stream of nitrogen. The organically functionalized substrate was incubated for 10 min in a solution containing 5 nm Au nanoparticles capped with dodecylamine (5 mg) dissolved into toluene (10 ml). After Au nanoparticle assembly, the substrate was rinsed with toluene, followed by ethanol, and again dried under a stream of nitrogen. This assembly process was repeated in a cyclic manner until five total layers of octanedithiol and Au nanoparticles were assembled.

4.4.2. Electrical measurements

After assembly, the substrates were electrically again characterized using a Hewlett Packard Semiconductor Parameter Analyzer Model 4156A. The current at +1 V had increased from 70 fA to 200 μA, a significant change when compared to the initial electrical values taken before assembly. Before- and after-assembly $I(V)$ curves are shown

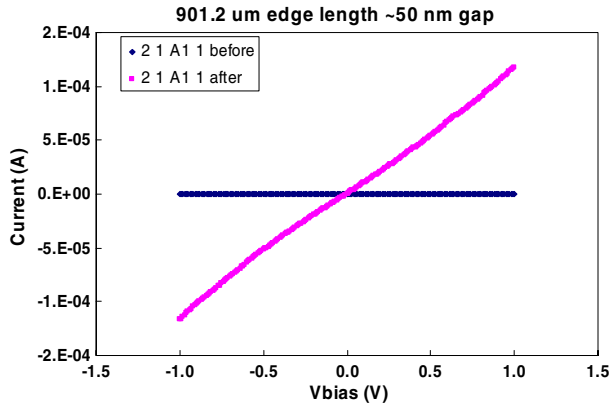

Figure 16. An example of the $I(V)$ curves before and after the octanedithiol and 5 nm Au nanoparticles are assembled into the nanogap.

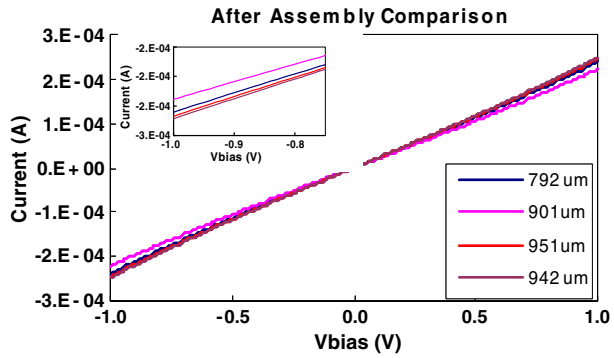

Figure 17. Graph showing the $I(V)$ responses of four devices having edge lengths of 792, 901, 942, and 951 μm. The inlaid graph is an expanded region of the graph from -1 to -0.7 V.

in figure 16. The origin of the nonlinear behaviour is still under investigation.

These assembly experiments were performed on 17 structures with 65% of all structures exhibiting similar behaviour, as illustrated in figure 17. The structures that did not have $I(V)$ characteristics as shown in figure 17 were shorted. Initial results indicate that the current increases as the edge length is increased.

Control experiments on gaps that excluded nanoparticles from the assembly steps showed no increase in electrical current. Furthermore, control experiments in which no organic, bi-functional cross-linker molecules were present in the toluene solution similarly showed no increase in current.

4.5 Conclusion

In conclusion, the authors have demonstrated a simple and effective method to produce 1D nanogaps using conventional photolithography and metal evaporation techniques. We have further demonstrated that the 1D nanogaps can be functionalized with Au nanoparticles and organic bi-functional cross-linker molecules.

Acknowledgment

Sandia is a multiprogram laboratory operated by Sandia Corporation, a Lockheed Martin Company, for the United States Department of Energy under contract DE-AC04-94AL85000.

References

[1] Reed M A, Zhou C, Muller C J, Burgin T P and Tour J M 1997 *Science* **278** 252–4
[2] Zhou C, Muller C J, Deshpande M R, Sleight J W and Reed M A 1995 *Appl. Phys. Lett.* **67** 1160–2
[3] Strachan D R, Smith D E, Johnston D E, Park T H, Therien M J, Bonnell D A and Johnson A T 2005 *Appl. Phys. Lett.* **86** 043109/1–3
[4] Janes D B, Ghosh S, Choi J, Lodha S and Bhattacharya S 2003 *IEEE Int. Conf. on Application Specific Systems, Architectures and Processors* (Piscataway, NJ: IEEE) pp 125–31
[5] Chen J, Reed M A, Rawlett A M and Tour J M 1999 *Science* **286** 1550–2
[6] Lambert M F, Goffman M F, Bourgoin J P and Hesto P 2003 *Nanotechnology* **14** 772–7
[7] Guillorn M A, Carr D W, Tiberio R C, Greenbaum E and Simpson M L 2000 *J. Vac. Sci. Technol.* B **18** 1177–81
[8] Lefebvre J, Radosavljevic M and Johnson A T 2000 *Appl. Phys. Lett.* **76** 3828–30
[9] Yun M H, Myung N V, Vasquez R P, Lee C S, Menke E and Penner R M 2004 *Nano Lett.* **4** 419–22
[10] Li C Z, He H X and Tao N J 2000 *Appl. Phys. Lett.* **77** 3995–7
[11] Chopra N, Xu W, Long L E D and Hinds B J 2005 *Nanotechnology* **16** 133–6
[12] Howell S W, Dirk S M, Childs K, Pang H, Blain M, Simonson R J, Tour J M and Wheeler D R 2005 *Nanotechnology* **16** 754–8
[13] Daniel L B, Leff V and Heath J R 1996 *Langmuir* **12** 4723–30

5. Potential Directed Assembly of Aryl Iodonium Salts onto Silicon {100} Hydride Terminated and Platinum Surfaces

Shawn M. Dirk[†], Svitlana Pylypenko[§], Stephen W. Howell[†], Julia E. Fulghum[§], David R. Wheeler[†]*

[†] Micro-Total Analytical Systems, Sandia National Laboratories, Albuquerque, NM, USA. [§]Department of Chemical and Nuclear Engineering, University of New Mexico, Albuquerque, NM, USA

RECEIVED DATE (automatically inserted by publisher); Add Author E-mail Address Here

5.1 Introduction

This communication describes the use of iodonium salts in an electro-reductive assembly process for the formation of organic mono- and multilayers onto silicon {100} that have been hydride passivated and platinium surfaces. Many publications have described the utility of aryl diazonium salts in electro-grafting assembly processes for the formation of organic mono- and multilayers on semi-conducting[1-4] and conducting surfaces.[5-10] Recently diazonium salts have been shown to self assemble without the use of potential on silicon, gallium arsenide and palladium surfaces.[11] Most recently iodonium salts have been assembled onto glassy carbon using electrochemical reduction.[12] We began to examine the use of iodonium salts because we desired the ability to easily pattern organic molecules onto silicon and metal surfaces in order to explore novel sensing platforms.

In our hands, numerous diazonium salts were easily assembled onto silicon and Pt surfaces, however, the diazonium assembly proved difficult to control when we attempting to direct the film assembly to particular regions of the substrate. Initially we evaluated the use of patterned n+ regions on a p type silicon substrate. While we were unable to stop assembly of the diazonium salts on the p type regions we observed enhanced assembly on the n+ regions. We were able to inhibit diazonium assembly on silicon surfaces with the use of positive bias. Retarded assembly was accomplished by first applying a positive bias of 2.0 V to a silicon substrate via a micro-alligator clip and then immersing the freshly hydride passivated silicon surface into a solution of 1.0 mmol/L diazonium salt dissolved in 0.1 M tetrabutylammonium tetrafluoroborate in acetonitrile with a platinum counter electrode. This technique is, however, less desirable for patterning applications than a technique that relies on direct writing with negative bias. Additionally, there are significant issues associated with maintaining a positive bias during the rinsing. Removal of bias results in assembly of the diazonium molecules.

As our search progressed for an organic film precursor that could be directed to assemble on specific regions of silicon while not assembling on others, we were drawn to the iodonium salts because the reduction potentials of similar salts are on the order of one volt more negative than the corresponding diazonium salts as determined by cyclic voltammetry.[13]

Initial assembly experiments were performed using a two electrode system in which a freshly hydrofluoric acid (15:1) treated silicon {100} substrate was clipped via a micro-alligator clip to a voltage source that supplied -2 V. The substrate was lowered into a solution of 1.0 mmol/L of iodonium salt dissolved in a 0.1 mol/L solution of tetrabutylammonium tetrafluoroborate dissolved in acetonitrile. Extreme care was taken to not immerse the micro-alligator clip in the assembly solution. The counter electrode was a platinum wire. The electro-grafting process was carried out for 10 min at ambient temperature. No special care was taken to exclude oxygen during the assembly process. After assembly the substrate was sonicated in fresh acetonitrile for 30 seconds, rinsed with ethanol and dried under a stream of nitrogen. The configuration for the assembly process is displayed in Figure 18.

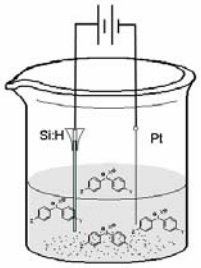

Figure 18. Iodonium assembly procedure in which an iodonium salt is dissolved in a solution of 0.1 mol/L Bu_4NBF_4 in CH_3CN and negative bias is applied for 10 min.

Several molecules ranging from electron deficient to electron rich were electro-grafted in this fashion. After assembly ellipsometry was used to determine the thickness of the molecular layer on the substrate. The results are shown in Table 1. The electron rich iodonium salts were shown to assemble thicker films than the electron deficient iodonium salts. Work is currently underway to fully understand this trend.

Table 1: Organic film thickness after assembly at -5 V and -2 V

Molecule	Measured Thickness (-5 V)	Measured Thickness (-2 V)	Calculated Thickness†
1 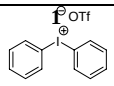	2.40 ± 0.07 nm	0.45 ± 0.21nm	0.46nm
2 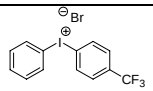	1.80 ± 0.18 nm	0.22 ± 0.08 nm	0.46 nm
3 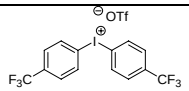	2.36 ± 0.13 nm	0.16 ± 0.04 nm	0.56 nm
4 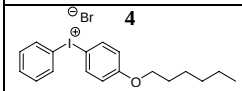	9.13 ± 1.50 nm	4.23 ± 1.70 nm	1.14 nm
5 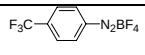	----	0.33 ± 0.22 nm*	0.54 nm

*Assembly of the diazonium was used as a control and was accomplished without the use of bias. †Calculated monolayer thickness was determined using Chem 3D software assuming that the molecules were replacing the hydride on the silicon {100} hydride surface.

X-ray photoelectron spectroscopy (XPS) was used to characterize molecules **2-5** immediately after assembly. C 1s and F 1s photoelectron peak shapes and binding energies confirm the presence of molecules **2, 3** and **5**. The experimentally determined C/F ratios are compared to theoretical ratios in Table 2. The measured ratios are slightly higher than the expected ratios, as a result of hydrocarbon contamination on the Si substrates. Corrections based on estimates of hydrocarbon contamination indicate that the trifluoromethylphenyl group is primarily deposited onto the surface from molecule **2**. The C1s photoelectron spectra, including the associated shake-up features, confirm the presence of molecule **4**. Silicon and oxygen from the substrate were detected in all cases, indicating that the assembled layers are thin. No attempt was made to correlate XPS and ellipsometry measurements, as variations in F/Si ratios demonstrate that layer thickness varies from area-to-area on the films. Films assembled from molecules **2** and **4** were reanalyzed two months after preparation. Small changes in elemental composition, primarily due to a slight increase in surface oxygen concentration, were observed. C1s and F1s photoelectron peak shapes remained consistent with the presence of the molecules.

Table 2: XPS data for assemblies prepared with molecules containing Fluorine

Molecule	XPS C/F(experimental)	C/F (theoretical)
2	3.7	4.3 or 2.3 *
3	4.0	2.3
5	2.6	2.3

*2.3 Corresponds to the transfer of only the trifluoromethylphenyl group of the iodonium salt to the surface as opposed to the transfer of both phenyl and trifluorphenyl groups.

Control experiments carried out without bias and the electrolyte failed to generate an organic film deposition as determined by ellipsometry. The same control experiment carried out with diazonium salt **5** resulted in the formation of a monolayer of self-assembled molecular film. When oxide passivated silicon was used as the substrate no assembly was observed for diazonium or iodonium salt.

We were able to use iodonium salt **1** to assemble[14] on a platinum substrate selectively in the presence of another platinum substrate by directly applying bias to one of the platinum lines an not the other platinum line. This assembly is shown in the false color image and histogram shown in figure 19.

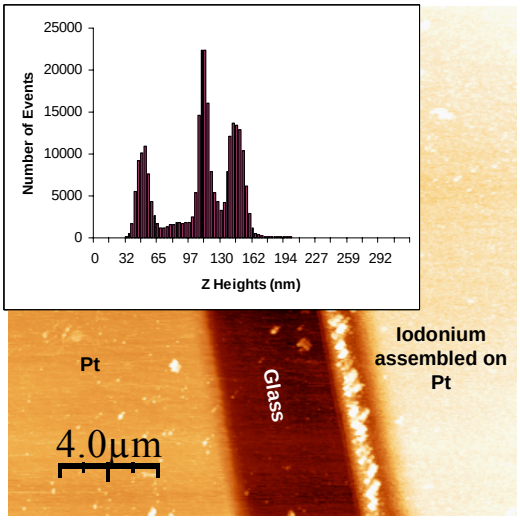

Figure 19. False color image of a 20 x 20 micron image captured via AFM with a histogram inlayed showing the directed assembly of iodonium salt. The brighter color has a higher topography in this image.

We propose that the mechanism of assembly is analogous to the method proposed by Stewart et al.[11] for the attachment of diazonium salts to silicon hydride terminated surfaces. In the first step of the reaction mechanism an electron is transferred from the surface of the silicon to the iodonium salt. A cleavage of the carbon iodine bond would result in a radical and iodobenzene. The radical can then be combined with the surface forming a silicon-carbon bond.

We believe that the reactive species is the iodonium salt and not the co-generated iodobenzene. Assembly experiments were performed in order to electro-graft iodobenzene (1.0 mmol/L) in Bu_4NBF_4 (0.1 M) to silicon {100} surfaces that have been freshly treated with a dilute HF solution. None of the experiments resulted in the formation of an organic film as measured by ellipsometry.

In conclusion we have developed a novel technique for the electro-grafting of iodonium salts on to silicon hydride terminated surfaces and Pt surfaces. This procedure provides a method for the bias driven and bias direct patterning of organic molecules onto platinum surfaces.

Acknowledgement: Sandia is a multiprogram laboratory operated by Sandia Corporation, a Lockheed Martin Company, for the United States Department of Energy under contract DE-AC04-94AL85000. The authors would like to thank Kent Childs, Matt Blain, Joe Simonson, and Tony Ohlhausen for help with substrate implantation and SIMS data collection.

Supporting Information Available: The details of the synthesis of compounds **1-5** and a detailed electro-grafting procedure and the XPS experimental data are available. Diazonium assembly procedures and SIMS data showing enhanced assembly of diazonium salt on n+ patterned surfaces is also available. This material is available free of charge via the Internet at http://pub.acs.org.

References

(1) Allongue, P.; de Villeneuve, C. H.; Cherouvrier, G.; Cortes, R.; Bernard, M. C. *Journal of Electroanalytical Chemistry* **2003**, *550-551*, 161-174.
(2) Hartig, P.; Dittrich, T.; Rappich, J. *Journal of Electroanalytical Chemistry* **2002**, *524-525*, 120-126.
(3) Allongue, P.; de Villeneuve, C. H.; Pinson, J. *Electrochimica Acta* **2000**, *45*, 3241-3248.
(4) Allongue, P.; De Villeneuve, C. H.; Pinson, J.; Ozanam, F.; Chazalviel, J. N.; Wallart, X. *Electrochimica Acta* **1998**, *43*, 2791-2798.
(5) Bahr, J. L.; Yang, J.; Kosynkin, D. V.; Bronikowski, M. J.; Smalley, R. E.; Tour, J. M. *Journal of the American Chemical Society* **2001**, *123*, 6536-6542.
(6) Boukerma, K.; Chehimi, M. M.; Pinson, J.; Blomfield, C. *Langmuir* **2003**, *19*, 6333-6335.
(7) Chausse, A.; Chehimi, M. M.; Karsi, N.; Pinson, J.; Podvorica, F.; Vautrin-Ul, C. *Chemistry of Materials* **2002**, *14*, 392-400.
(8) Bravo-Diaz, C.; Romero, E. G. *Current Topics in Electrochemistry* **2003**, *9*, 27-46.
(9) Brooksby, P. A.; Downard, A. J. *Langmuir* **2004**, *20*, 5038-5045.
(10) Marcoux, P. R.; Hapiot, P.; Batail, P.; Pinson, J. *New Journal of Chemistry* **2004**, *28*, 302-307.
(11) Stewart, M. P.; Maya, F.; Kosynkin, D. V.; Dirk, S. M.; Stapleton, J. J.; McGuiness, C. L.; Allara, D. L.; Tour, J. M. *Journal of the American Chemical Society* **2004**, *126*, 370-378.
(12) Vase, K. H.; Holm, A. H.; Pedersen, S. U.; Daasbjerg, K. *Langmuir* **2005**, *21*, 8085-8089.
(13) Cyclic voltammetry of benzene diazonium tetrafluoroborate in DMF with 0.1 M Bu4BF4 with a Pt/Pt/Ag-AgNO3 electrode system showed a reduction peak at -0.5 V at a sweep rate of 10 mV/s. Trifluoromethanesulfonatediphenyl-iodonium had a reduction peak at -1.5 V under the same conditions.
(14) The iodonium salt was assembled by pulsing the voltage (-2V) on and off for 30 cycles to build a thick layer that was easily seen with AFM.

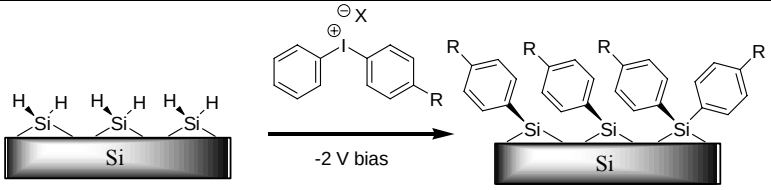

A novel electro-graft method of forming covalent bonds directly to silicon hydride or platinum surfaces has been demonstrated with the use of iodonium salt precursors. Initially a silicon substrate is treated with a dilute hydrofluoric acid wash to ensure a hydride passivated surface which is immersed in a solution of iodonium salt dissolved in a solution of tetrabutylammonium tetrafluoroborate in acetonitrile. Grafting is accomplished by applying a negative bias to the silicon substrate. Directed assembly has been demonstrated with Pt substrates.

6. Additional info for the ESC section:

After initially observing an acid-base induced conductance shift, several experiments were conducted to determine the longevity of the conductance switching in liquid phase.

A robotic dipper was used to systematically expose the nanoparticle films to solutions of acid and then base, while measuring the films resistance after a predetermined drying time. A representative result from these experiments is shown in Figure 20 and 21.

Figure 20 shows data collected for a Au nanoparticle film crossed-linked with mPE nitro phenol. During the early stages of exposure, film clearly switches between conduction states. However, after several switching cycles, the change in conductance becomes undetectable. Figure 21 shows a controlled film of Au nanoparticles crosslinked with ODT. When exposed to acid/base, the ODT linked films show no switching behavior.

The degradation of the molecular switching shown in figure 20 is believed to be caused by acid catalyzed benzofuran formation (figure 22). When the sensing molecules become trapped in this structural configuration they no longer can chemically be deprotonated and are trapped into a fixed electronic state. These experiments were very useful for determining the appropriate changes required to design molecules that are not susceptible to the catalyzed formation.

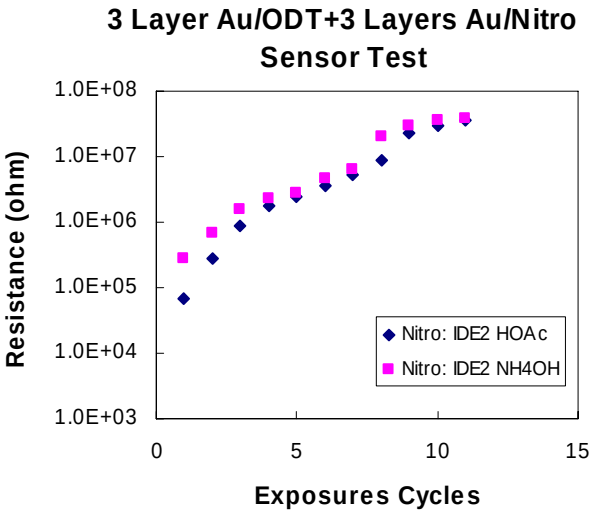

Figure 20

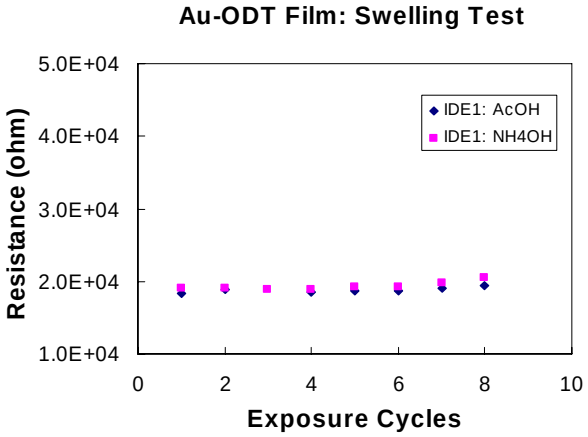

Figure 21

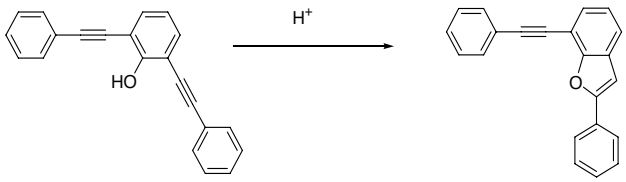

Figure 22

Vapor Sensing Data

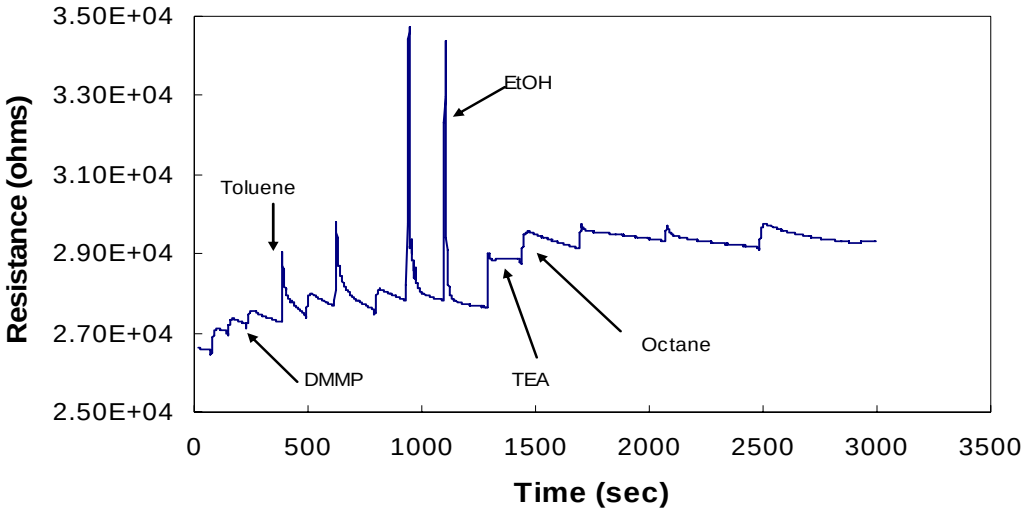

Figure 23

Figure 23 displays vapor sensing data of a Au nanoparticle film cross-linked with mPE nitro phenol. For this experiment, the nanoparticle film was placed into a home-built vapor cell in which various analytes flowed across the nanoparticle film while its resistance was measured. The vapor sources used for the experiment were vials that contained solutions of the analytes at room temperature. The consternations of the various analytes are related to the vapor pressure of the individual analyte. For this experiment the concentrations of most of the analytes were ~ 1%.

Figure 24 highlights the portion of the experiment shown in Figure 23 where the nanoparticle film was exposed to DMMP, toluene and ethanol. This data clearly shows behavior differences when the film is exposed to an analyte which deprotonates the nitro phenol molecule and analytes which causes swelling of the film such as toluene and ethanol. When the film is exposed to DMMP and TEA (analytes that deprotonate the mPE molecule), there appears to be a permanent modification to the film's conductance compared to toluene and ethanol. The modification is evident in the increasing offset after each exposure to DMMP and TEA (Figure 23). Another interesting aspect of the data shown in figure 24 is the relative sizes of the resistance changes during exposure. The different changes are related to the varying concentrations of the different analytes, where these concentrations are related to the analyte's vapor pressure. The vapor pressure of DMMP at room temperature is 1.4 mmHg, while for toluene it is 28.4 mmHg. Therefore the concentration of DMMM is ~ 20 times less than toluene. From the recorded data, the relative change in the resistance of the film when exposed to DMMP is 500Ω compare to that of toluene 1600Ω. Therefore the DMMP transduction signal is ~ 3 times less than the signal for the toluene. This data suggests that if this film was exposed to vapors of DMMP and toluene at the same concentration, the film would be more sensitive to the DMMP. Producing films with increased selectivity to analytes such as

DMMP would be a major improvement in the development of nanoparticle based sensors.

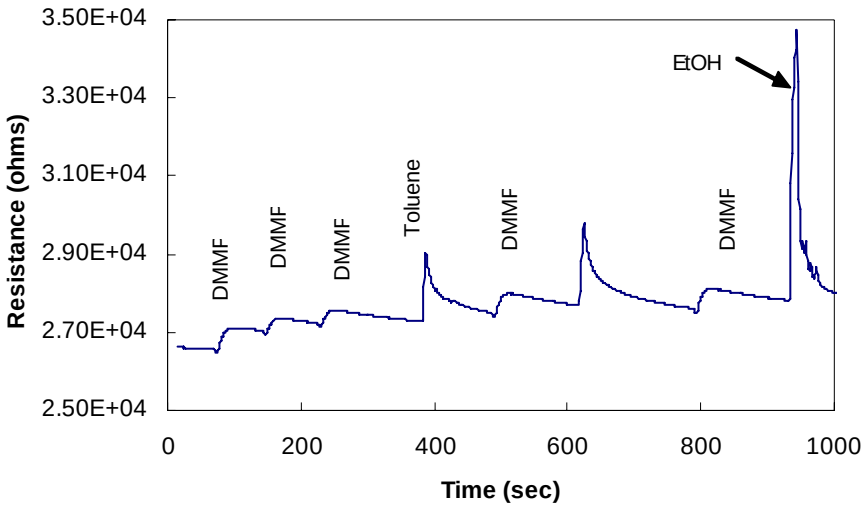

Figure 24

7. MODIFICATION OF NANOPARTICLE-ORGANIC COMPOSITE ELECTRONIC MATERIALS FOR IMPROVED CHEMICAL SENSORS

Stephen W. Howell, Shawn M. Dirk and David R. Wheeler
Sandia National Laboratories
Micro Total Analytical Systems Department
Albuquerque, NM 87185-0892 (USA)

Molecular electronic based chemical vapor sensors were assembled using noble metal nanoparticles and short conjugated phenylene ethynylene (PE) based molecules. Sacrificial capping ligands on the nanoparticles were replaced by tighter binding PE ligands. The films were assembled between pairs of electrodes by iteratively exposing the substrates to solutions of the nanoparticles and PE crosslinking bridging ligands. Some of the conjugated bridging molecules contained an electron deficient phenol to provide a simple platform for developing sensor applications. The phenol is calculated to have a significant change in its HOMO/LUMO gap in the presence of specific analytes. Judicious combination of nanoparticle size and ligand structure provides a film in which the organic bridging ligands dramatically affect film conductance. Specifically, π-conjugated ligands lower resistance more in films with smaller nanoparticles. Thus the sensing mechanism of these films is not based on the typical swelling mechanism but rather on the modulation of the molecular electronic structure of the conducting PE bridging ligands.

7.1 INTRODUCTION

Recently, thin films composed of nanoparticles have emerged as useful chemical sensor platforms. Wohltjen *et al.* have demonstrated the ability to sense various chemical agents with a sensitivity in the part per million volume (ppmv) range (2). In these systems, the transduction mechanism is based on a swelling of the film. Swelling, though very sensitive, typically lacks chemical specificity. While modified nanoparticle films have been prepared, they still rely on a swelling mechanism. The goal of our work is to develop complimentary signal transduction methods that may provide more information about the analyte via specific interactions with the organic portions of the nanoparticle network.

In order for sensors based on nanoparticle films to become a practical sensing platform, the issue of chemical specificity must be addressed. Our approach of using designer conductive organic cross-linking molecules arrayed between nanoparticles is a departure from the typical swelling based systems that have been examined. We have designed and synthesized conjugated molecules, which have an electron deficient phenol as the central component of the molecule. Electron poor phenols bind phosphonates via

an acid/base hydrogen bonding interaction. Phosphonates are of particular interest as they provide good models for chemical warfare agents. Prior to sensing evaluations of phosphonates, we chose to evaluate our system with a much simpler direct acid base interaction. As the binding event occurs with the analyte, the conductivity path is modified and the presence of an analyte is determined via an electrical transduction mechanism.

7.2 EXPERIMENTAL SECTION

7.2.1 Sample Preparation

Gold interdigitated electrodes (IDE) built on quartz substrates were first silanized with a solution of tetrakis(dimethylamino)silane in toluene. The remaining amino functionalities were displaced with 1,8-octanedithiol (ODT) from a toluene solution to give a thiolated surface capable of binding nanoparticles. The substrate was then incubated in a solution of dodecylamine-capped metal nanoparticles dissolved in toluene or hexane (4). The film thickness was increased via alternating exposure to solutions of bifunctional crosslinking molecules and nanoparticles (Figure 25). The nanoparticles used for these studies employed 5 nm gold and 2 nm platinum particles.

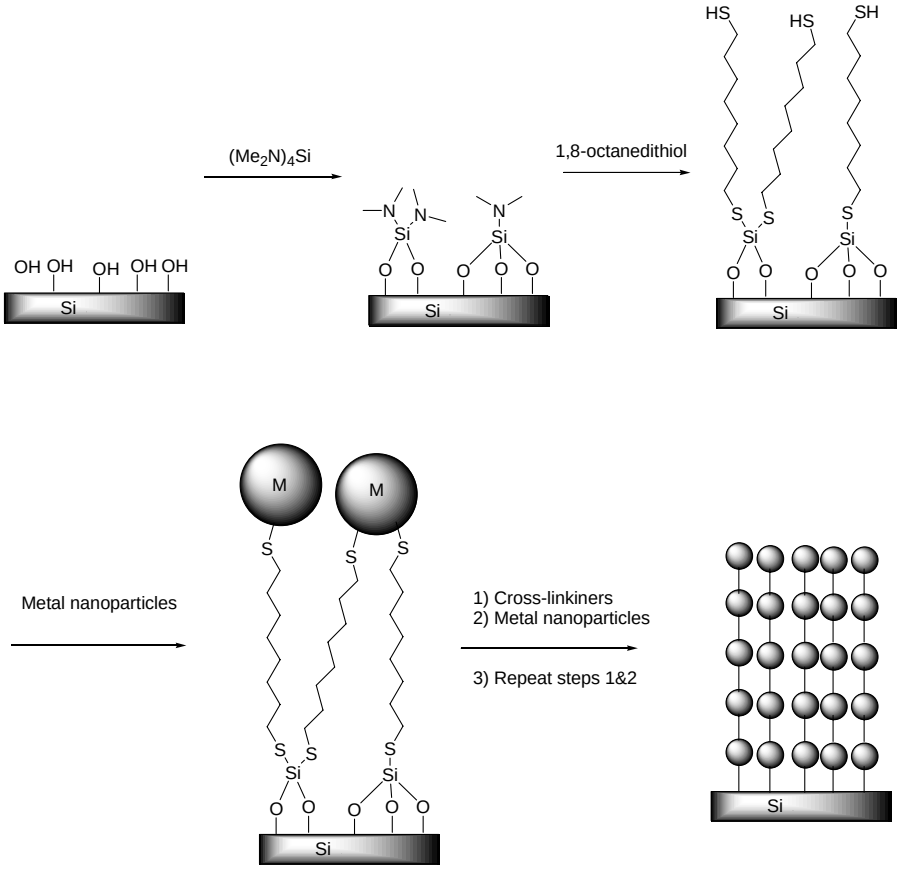

Figure 25. Schematic of sample preparation.

Numerous other techniques exist for the deposition of nanoparticle films, such as controlled pulling (5), or the use of charged polymers and charged nanoparticles, or slow incubation of thiol capped nanoparticles in dithiol solution. However, we use the unique

chemistry described above in conjunction with a robotic sample preparation system to deposit nanoparticle films of different thickness on prepared electrodes in a very reproducible manner.

The robotic system consists of a precision linear stage oriented vertically above a rotary stage. Vials containing the various materials used to build our films are pre-positioned on the circular table connected to the rotary stage. To expose the IDE sample to any particular chemistry, the vial containing that solution is rotated to a position under the vertically mounted linear translation stage. The IDE sample, mounted to a vacuum chuck, is lowered into the solution for a preset amount of time. After exposure, the sample is raised from the solution and positioned vertically in line with a filtered N_2 blower that is used to dry the sample. After drying, the rotary stage positions the next solution used to build the film. Rinsing steps are included between the exposure to the nanoparticles and crosslinker solutions.

To iteratively build our films, we use the following 7 steps: 1) An IDE, which has been functionalized with the appropriate surface linking chemistry, is submerged in a nanoparticle solution for 5 minutes; 2) The IDE sample is then removed from the nanoparticle solution, and then dried and submerged into a toluene solution for rinsing; 3) The IDE sample is removed from the toluene, dried and submerged into ethanol for additional rinsing; 4) After the ethanol rinse, that IDE sample is dried and submerged into a solution of a cross-linking molecule (such as ODT (octane dithiol) or *m*-PE diisocyanide (*meta*-bis(4-isocyanide phenylethynyl)benzene); 5) and 6) The sample is removed from the cross-linker and is rinsed in toluene and then ethanol (same as steps 2 and 3); 7) After rinsing, the IDE sample is resubmerged into the nanoparticle solution (thus building the next layer). By repeating steps 1-7, nanoparticle films of any thickness can be deposited.

The robotic sample preparation system also has the ability to measure the resistance of the nanoparticle film after the assembly of each layer. This is possible because the IDEs used for these experiments have large, well-placed contact electrodes. A custom translation jig is used to hold two pogo pins with a spacing that mates with the contact electrodes of the IDE. The pogo pins are brought into contact with the IDE's electrodes using a solenoid. The solenoid is activated by a general-purpose interface bus (GPIB) controlled power supply. To measure the film's resistance, the voltage source of a Keithley 6487 is connected to one of the pogo pins. The current input of the 6487 is connected to the other pogo pin. The I(V) characteristics of the film are measured by ramping the voltage source of the 6487 (also controlled via GPIB). The film resistance is determined by fitting the measured I(V) curve.

A LabVIEW™ program controls the entire operation of the robotic system. The program was designed to use a recipe file to control the process of assembling and measuring the properties of the nanoparticles. This approach makes for a very versatile sample preparation system.

By preparing the nanoparticle films using a robot, problems associated with irregularities of the deposited films were eliminated. This sample preparation system was designed with the capability to measure the resistivity of the nanoparticle films after assembly of each layer. Use of such a sample preparation system is vital for developing mass-produced sensors from nanoparticle films and gathering statistics on device performance.

7.2.2 Sample Characterization

Nanoparticles and assembled films were characterized by TEM and AFM prior to electrical characterization. Figure 26 shows an AFM image of a gold electrode on a quartz surface before and after the assembly of 5 Au nanoparticle layers. For this experiment, only Au attachment chemistry was used (no chemical binding to the underlying quartz substrate). Figure 26b clearly displays an ~ 20 nm increase in the topographic height of the gold electrode (relative to the quartz surface) after the iterative assembly. The accompanying histograms (Figures 26c and 26d) show a dramatic increase in both the topographic height and the roughness of the gold electrode. This is expected since it is unrealistic to expect a crystal-like assembly of each nanoparticle layer.

Figure 27 shows high-resolution cross-sectional SEM images of a gold and platinum nanoparticle films assembled onto a gold IDE substrate. The SEM image of the deposited Au film clearly shows the presence of thin nanoparticle films draped across the Au electrode of the IDE. However, there are numerous Au agglomerations present on the surface of the IDE. There are many possible explanations for these agglomerates and we are working to determine their origin. A likely explanation is that the nanoparticle solution slowly develops agglomerated particles from cross contamination. Resistances vs. thickness measurements for multiple film samples made from Au nanoparticles (see below) show very little variance. Therefore, we believe these agglomerations do not dramatically affect the electrical D. C. conduction of the film. Figure 27 27 shows very few nanoparticle agglomerations on the surface of the deposited Pt film.

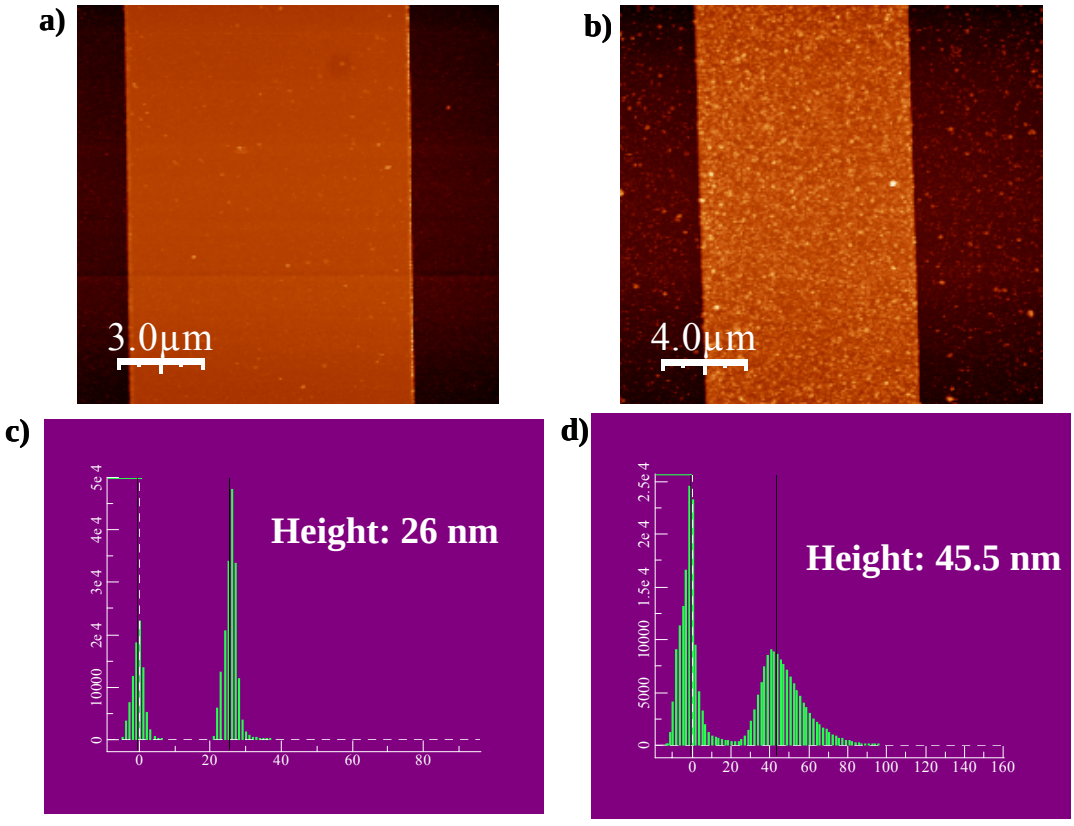

Figure 26. AFM image of a gold electrode on a quartz wafer a) before assembly and b) after 5 iterations of 1,8-octanedithol and Au nanoparticles. c) and d) are accompanying histograms for a) and b) respectively. The

histograms show a dramatic increase in the height of the Au line after the assembly.

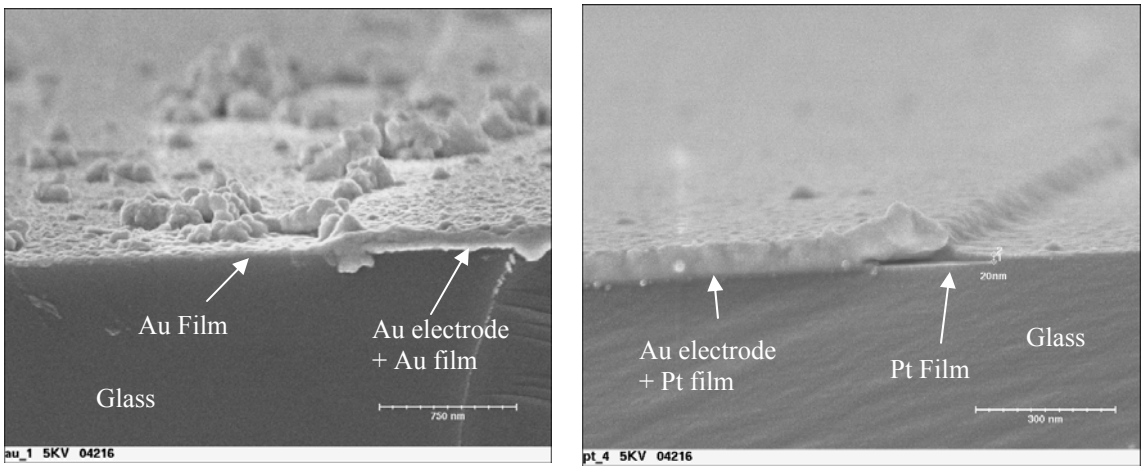

Figure 27. Cross-sectional SEM images of Au and Pt nanoparticle films deposited on a gold IDE.

RESULTS AND DISCUSSION

7.2.3 Nanoparticle Film Assembly Results

The robotic system, described above, was used to deposit and measure the electrical properties of Pt and Au nanoparticle films linked with different ligands such as ODT and *meta*-PE diisocyanide. Figure 28 is a plot showing the resistance vs. number of deposited film layers for several combinations of nanoparticles and bridging crosslinker-ligands. The data demonstrates that the resistance of the films decreases and eventually saturate as additional nanoparticle layers are deposited. The saturation occurs when no new additional low-resistance current paths are added during the assembly of a new nanoparticle layer. There is also an inversion in the resistance per layer that depends on the nanoparticle's type and the ligand used to crosslink the film. The data show that a film composed of 2 nm Pt nanoparticles linked with ODT has a higher resistance than a Pt film linked with *m*-PE Diisocyanide. The *meta*-PE Diisocyanide is potentially a conductive bridging molecule due to its pi-conjugation. However, for films composed of 5 nm Au nanoparticles, the opposite conductivity pattern is realized. The shorter non-conjugated ODT ligand provides for a more conductive film. This observation is significant because it shows that the selection of certain nanoparticle properties (such as size and material) and selection of an appropriate linking ligand can be used to tune the conductance and presumably the conductance mechanism of a nanoparticle-ligand composite film.

Modification of the conduction of Au nanoparticle films, utilizing different linker ligands, was recently observed by Wessels *et al.* (6). However, we also see a dependence on nanoparticle size and composition. It is well known that smaller nanoparticles have a higher charging potential (7-10). This, coupled with the inherent variability and tunability of an organic molecule's electrochemical potential, ensures that a film in which the organic molecules dominate conductivity can be achieved. In many respects the films

that we are generating can be thought of as a conducting polymers (or oligomers) interconnected by a nanoparticle scaffold.

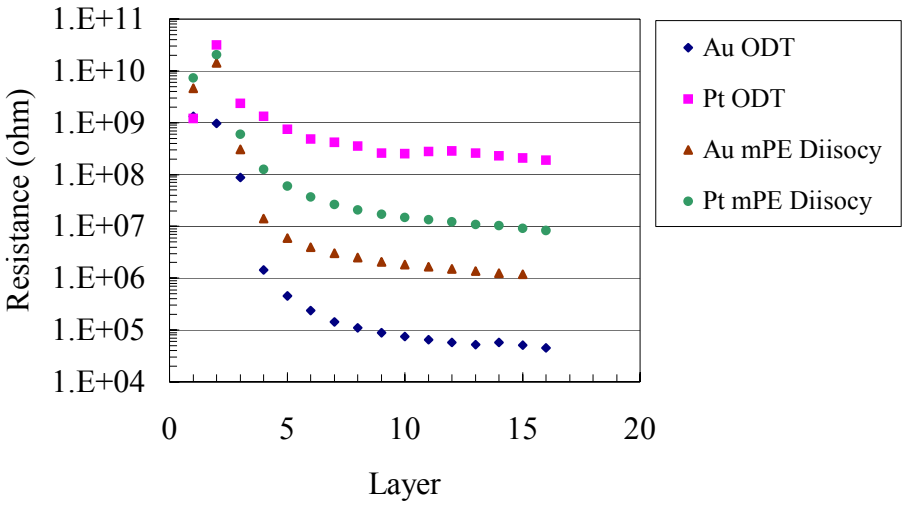

Figure 28. Resistance vs. layer data for several combinations of nanoparticles and linker molecules.

7.2.4 Nanoparticle Film Initial Sensing Results

In addition to the experiments above, nanoparticle films were assembled using cross-linkers that can interact with an analyte in such a manner as to change the bridging molecule's HOMO/LUMO gap. The cross-linker used was a conductive phenylene ethynylene molecules containing nitrophenol functionality as the central component, *meta*-bis(4-isocyanide phenylethynyl) *para*-nitrophenol. The conjugated molecule was synthesized using Sonogashira coupling chemistry (11). The nanoparticles used were dodecylamine capped gold nanoparticles (4).

Figure 29 shows a typical I(V) curve for Au nanoparticles crosslinked with *meta*-bis(4-isocyanide phenylethynyl) *para*-nitrophenol, a phenylene ethynylene based electron deficient phenol. There is a clear, reversible change in the resistance of the film when exposed first to acid and then base. This observed switching is consistent with the organic crosslinking molecule changing between cross-conjugated and fully conjugated states as the assembly is dipped into base and acid, respectively. Because the organic moiety plays a smaller role in the conduction mechanism of films made with the larger gold nanoparticles, it is expected that the same experiment employing the smaller platinum nanoparticles will provide for an even larger effect. The generation of this new response mechanism for nanoparticle films greatly increases the scope of organic/nanoparticle films for sensor applications. The crosslinked nature of these nanoparticle-ligand composite films increases their robustness relative to similar films made with nonfunctional ligands, and should allow for their use in aqueous and organic solvents in addition to their use as vapor sensors.

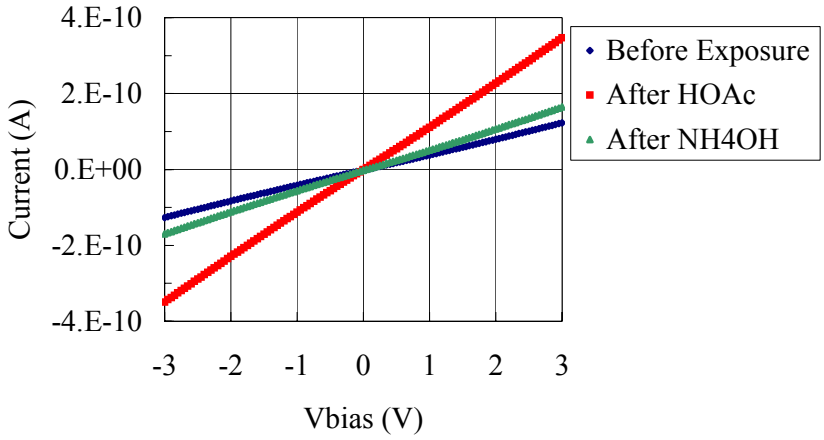

Figure 29. Typical I(V) curves of a nanoparticle film before and after sequential exposures to HOAc and NH_4OH. There is a reversible change in the resistance of the film.

7.3 CONCLUSION

In summary, we have developed a sample preparation system that enables very reproducible deposition of crosslinked nanoparticle films on a variety of substrates. This system has the ability to acquire electrical data during sample deposition. Data collected for several nanoparticle film depositions demonstrates our ability to vary the conduction mechanism and the total conduction of the film by the selection of nanoparticle size, composition, and the cross-linking ligand. The material we have developed is a hybrid intermediate between a true organic conducting polymer and a classical nanoparticle film. The nanoparticles provide a scaffold on which to assemble various conducting/sensing oligomers and ligands.

ACKNOWLEDGMENTS

The authors would like to thank Dr. Robert Simonson, Dr. Matthew Blain, Dr. Kent Childs and Sherry Zmuda for their useful conversations. Sandia is a multiprogram laboratory operated by Sandia Corporation, a Lockheed Martin Company, for the United States Department of Energy under contract DE-AC04-94AL85000

REFERENCES

1. N. S. Lewis, B. J. Doleman, S. Briglin and E. J. Severin, *U.S. 6537498*, 24 pp. (2003).
2. H. Wohltjen and A. W. Snow, *Analytical Chemistry*, **70**, 2856 (1998).
3. H. L. Zhang, S. D. Evans, J. R. Henderson, R. E. Miles and T. H. Shen, *Nanotechnology*, **13**, 439 (2002).
4. N. Krasteva, B. Guse, I. Besnard, A. Yasuda and T. Vossmeyer, *Sensors and Actuators, B: Chemical*, **B92**, 137 (2003).
5. R. D. Tilley and S. Saito, *Langmuir*, **19**, 5115 (2003).
6. J. M. Wessels, H.-G. Nothofer, W. E. Ford, F. von Wrochem, F. Scholz, T. Vossmeyer, A. Schroedter, H. Weller and A. Yasuda, *Journal of the American Chemical Society*, **126**, 3349 (2004).
7. M. Aslam, I. S. Mulla and K. Vijayamohanan, *Applied Physics Letters*, **79**, 689 (2001).
8. P. E. Trudeau, A. Orozco, E. Kwan and A. A. Dhirani, *Journal of Chemical Physics*, **117**, 3978 (2002).
9. N. Fishelson, I. Shkrob, O. Lev, J. Gun and A. D. Modestov, *Langmuir*, **17**, 403 (2001).
10. T. Baum, D. Bethell, M. Brust and D. J. Schiffrin, *Langmuir*, **15**, 866 (1999).
11. K. Sonogashira, Y. Tohda and N. Hagihara, *Tetrahedron Letters*, 4467 (1975).

Distribution

Internal

1	MS-1078	S. Martin, 1720
1	MS-0892	R. Cernosek, 1722
1	MS-0603	M. Blain, 1722
10	MS-0892	S. Dirk, 1722
10	MS-0892	S. Howell, 1722
1	MS-0892	R.Simonson, 1722
10	MS-0892	D. Wheeler, 1722
1	MS-0603	S. Zmuda, 1722
1	MS-1084	K. Childs, 1748
1	MS-9018	Central Technical Files, 8945-1
2	MS-0899	Technical Library, 9616